Remote Sensing of Environment 177 (2016) 171–183

Contents lists available at ScienceDirect

Remote Sensing of Environment

journal homepage: www.elsevier.com/locate/rse

Reconstructing semi-arid wetland surface water dynamics through spectral mixture analysis of a time series of Landsat satellite images (1984–2011)

Meghan Halabisky [a,*], L. Monika Moskal [a], Alan Gillespie [b], Michael Hannam [c]

[a] School of Environmental and Forest Sciences, University of Washington, Seattle, WA, United States
[b] Department of Earth and Space Sciences, University of Washington, Seattle, WA, United States
[c] Smithsonian Environmental Research Center, Edgewater, MD, United States

ARTICLE INFO

Article history:
Received 8 August 2014
Received in revised form 4 February 2016
Accepted 17 February 2016
Available online 26 February 2016

Keywords:
Time series
Landsat
Wetlands
Hydrology
Hydroperiod
High resolution
OBIA
Object-based image analysis
Hydrograph
Monitoring
Sub-pixel

ABSTRACT

Wetlands are valuable ecosystems for maintaining biodiversity, but are vulnerable to climate change and land conversion. Despite their importance, wetland hydrology is poorly understood as few tools exist to monitor their hydrologic regime at a landscape scale. This is especially true when monitoring hydrologic change at scales below 30 m, the resolution of one Landsat pixel. To address this, we used spectral mixture analysis (SMA) of a time series of Landsat satellite imagery to reconstruct surface-water hydrographs for 750 wetlands in Douglas County, Washington State, USA, from 1984 to 2011. SMA estimates the fractional abundance of spectra representing physically meaningful materials, known as spectral endmembers, which comprise a mixed pixel, thus providing sub-pixel estimates of surface water extent. Endmembers for water and sage steppe were selected directly from each image scene in the Landsat time series, whereas endmembers for salt and wetland vegetation were derived from a mean spectral signature of selected dates spanning the 1984–2011 timeframe. This method worked well ($R^2 = 0.99$) for even small wetlands (<1800 m^2) providing a wall-to-wall dataset of reconstructed surface-water hydrographs for wetlands across our study area. We have validated this method only in semi-arid regions. Further research is necessary to extend its validity to other environments. This method can be used to better understand the role of hydrology in wetland ecosystems and as a monitoring tool to identify wetlands undergoing abnormal change.

1. Introduction

Wetlands are among the most biodiverse ecosystems in the world, due largely to their dynamic hydrology (Mitsch & Gosselink, 2007). The hydroperiod, which we define as the pattern of flooding and drying within a wetland, is the most important determinant in the establishment and maintenance of specific wetland habitat types and the species that they support (Babbitt, 2005; Correa-Araneda, Urrutia, Soto-Mora, Figueroa, & Hauenstein, 2012; Mitsch & Gosselink, 2007; Tavernini, Mura, & Rossetti, 2005). Despite the importance of the wetland hydroperiod, it is not well understood (Mitsch & Gosselink, 2007), in part because it is time-consuming and expensive to monitor changes in wetland hydrology using field measurements. Landscape-level hydroperiod data are scarce because tracking changes in wetland water levels over weeks and months requires the installation of expensive monitoring equipment or visiting sites many times a year for several years (Ryan, Palen, Adams, & Rochefort, 2014). However, without broad-scale long-term hydroperiod data it is not possible to adequately monitor changes in the hydrologic regime of wetlands to understand general patterns across different wetland types and to distinguish the difference between natural and abnormal changes to wetland hydrology. Furthermore, without adequate baseline data of the wetland hydroperiod, it is not possible to understand how changes in temperature and precipitation will impact the hydrology, structure and function of wetlands under climate change (Arnell et al., 2001; Poiani, Johnson, Swanson, & Winter, 1996; Ryan et al., 2014; Werner, Johnson, & Guntenspergen, 2013).

1.1. Wetland definition

We define wetlands using the United States Army Corps of Engineer's definition of wetlands as "those areas that are inundated or saturated by surface or ground water at a frequency and duration sufficient to support, and that under normal circumstances do support, a prevalence of vegetation typically adapted for life in saturated soil conditions." (Environmental Laboratory, 1987) Shallow lakes and lake fringes meet the above definition within our study area, and therefore, this analysis includes both large and small waterbodies.

* Corresponding author at: Box 352100, Seattle, WA 98195-2100, United States.
E-mail address: halabisk@uw.edu (M. Halabisky).

http://dx.doi.org/10.1016/j.rse.2016.02.040
0034-4257/

1.2. Remote sensing of wetland surface water dynamics

Remote sensing has provided a useful means to study the changes in wetlands through spatially explicit, cost- and time-effective data (Ozesmi & Bauer, 2002). However, mapping the hydroperiod of wetlands offers several challenges to remote-sensing analysts. The core challenge is the trade-off between temporal and spatial resolution of remotely sensed imagery. Currently, no one sensor has both the temporal and spatial resolution to detect the fine-scale patterns of wetland change over time, particularly for small wetlands (Gallant, 2015; Tiner, 2009; Wulder, Hall, Coops, Steven, & Franklin, 2014).

Landsat imagery with moderate spatial and temporal resolution has widely been used for surface water mapping through hard classification methods (sensu Foody, 2000), which classify pixels as either water or non-water. Commonly used classification methods include thematic classification, multi-band indices (e.g. normalized difference water index, NDWI (McFeeters, 1996)), single band thresholding, and spectral mixture analysis (Ozesmi & Bauer, 2002). These methods have been successfully applied to map surface water changes of large lakes and wetlands (Adams & Sada, 2014; Bryant & Rainey, 2002; Castaneda & Herrero, 2005; Hui, Xu, Huang, Yu, & Gong, 2008; Liu et al., 2013; Sener, Davraz, & Sener, 2010). However, wetlands that express changes in surface water extent at fine scales (below 30 m – the resolution of 1 Landsat pixel) and small wetlands, which we define as wetlands smaller than 5 ha, have received considerably less attention (Ryan et al., 2014). This is an issue because in many regions of the world the majority of the landscape is composed of small wetlands (Downing et al., 2014; Gilmer, Work, Colwell, & Rebel, 1980; Halabisky, Moskal, & Hall, 2011).

For high resolution mapping of wetlands analysts typically use high-resolution aerial imagery (<1 m), but repeat coverage is lacking (Tiner, 1990). This has limited high-resolution remote sensing of wetlands to detecting change between a few dates (Adams & Sada, 2014; Dyke & Wasson, 2005; Hui et al., 2008; Liu et al., 2013; Murkin, Murkin & Ball, 1997; Niemuth, Estey, Reynolds, Loesch & Meeks, 2006). Although useful, change detection of wetlands under these limitations does not provide enough detail for understanding patterns and dynamics of annual and inter-annual wetland response, much less to determine if measured changes in the surface water extent represent natural year-to-year variability, or abnormal changes in wetland hydrology. Even several dates of aerial imagery cannot provide enough information to determine the hydrologic regime of a particular wetland necessary for monitoring or future climate modeling.

In order to address this limitation several researchers have used one or more soft classification techniques such as multi-band indices and single band tracking to predict sub-pixel surface water estimates of Landsat imagery (Beeri & Phillips, 2007; Frohn et al., 2012; Gómez-Rodríguez, Bustamante, & Díaz-Paniagua, 2010; Huang, Peng, Lang, Yeo, & McCarty, 2014; Huang, Dahal, Young, Chander, & Liu, 2011; Reschke & Hüttich, 2014; Rover, Wylie, & Ji, 2010b). Soft classification methods do not assign a pixel to one class, but instead provide an estimate of class membership and can be used to measure the sub-pixel surface water area through regression modeling and classification and regression trees (Foody, 2000). However, these methods require a large amount of training data from field data or higher resolution imagery from the same time period and are not directly transferable to other study areas (but see Rover, Wylie, & Ji, 2010a).

Spectral mixture analysis (SMA) is a physically based technique which can be used to estimate the percent cover of surface water without the need for extensive training data. SMA estimates the fractional abundance of spectra representing physically meaningful materials, known as spectral endmembers, which comprise a mixed pixel, thus providing sub-pixel estimates of surface water extent (Adams, Smith, & Johnson, 1986; Adams & Gillespie, 2006). While SMA provides sub-pixel fractions of surface materials, it is commonly used to drive a classification by converting mixed pixels into water or non-water through selection of a threshold value (Shanmugam, Ahn, & Sanjeevi, 2006). Frohn et al. (2012) used SMA to identify wetlands at sub-pixels scales, but did not use it to estimate the percent cover of surface water or track changes to surface water through time.

While sub-pixel methods can identify the percent cover of surface water they do not provide the location of surface water within a pixel, which makes tracking change over time challenging. To remedy this issue, researchers have either tracked changes of individual pixels (Beeri & Phillips, 2007; Collins et al., 2014; Gómez-Rodríguez et al., 2010; Reschke & Hüttich, 2014) or summarized changes for all pixels within an entire landscape (Beeri & Phillips, 2007; Huang et al., 2014; Huang et al., 2011). Table 1 summarizes the key papers that meet one or more of the criteria necessary for high resolution mapping of wetland surface water dynamics.

What is almost entirely missing from the methods summarized in Table 1 is the ability to track changes to individual wetlands and the temporal detail to monitor both seasonal and long-term changes in wetland hydrology. Only one study that achieved this was Gómez-Rodríguez et al. (2010) in which the authors measured changes in the flooding duration of wetlands by examining how pixel reflectance of the near infrared band changed through time for over 800 temporary ponds spanning a 23-year time period in the Doñana National Park, Spain. Because the authors co-registered images to correct for small pixel misalignments between image scenes they could track changes of surface water extent for pixels within an individual wetland showing a significant trend of hydroperiod shortening likely due to groundwater depletion from agricultural irrigation. However, a challenge with tracking single pixels through time is the labor-intensive and imperfect process of pixel-to-pixel registration and atmospheric correction for multi-date analysis (Dai, 1998; Song, Woodcock, Seto, Lenney, & Macomber, 2001; Wyawahare, Patil, & Abhyankar, 2009). For some projects, it is not feasible to perform these pre-processing steps on hundreds of images.

We sought to develop a method that mapped surface water dynamics at temporal and spatial scales similar to Gómez-Rodríguez et al. (2010), but with minimal pre-processing. Additionally, we aimed to use this data to reconstruct individual wetland surface water hydrographs, which chart the pattern of flooding within a wetland over time. Here we use the term hydrograph to refer to temporal changes in surface-water extent (area) within a wetland, rather than temporal changes in water depth. This is due to the difficulty of determining water depth from a pixel composed of multiple surface materials.

The goal of this project was to develop a semi-automated tool to map and monitor wetland dynamics for individual wetlands while still covering a broad landscape. Specific objectives of this research were to:

1.) Develop a method with minimal pre-processing to estimate surface-water extent for wetlands at scales below 30 m.
2.) Reconstruct individual wetland hydrographs from 1984 to 2011.
3.) Determine if hydrographs could be used to classify wetland types and monitor wetland change over time.

2. Study area

We chose Douglas County, Washington (WA), located in the Columbia Plateau ecoregion in the Northwest of the United States as our study area (Fig. 1) as wetlands are abundant and representative of semi-arid ecosystems common to Western North America. Douglas County is 4714 km^2 in size with non-irrigated farming and ranching being the dominant land uses. It is a semi-arid sage steppe ecosystem, receiving an average of 29 cm of precipitation a year. Douglas County is bordered by the Columbia River with a low elevation of 180 m near the river and rising to an elevation of 1220 m at the top of the plateau. In general, the surface topography of the plateau is subtle and free from shadows resolved at the 30-m Landsat scale. Isolated, depressional wetlands are the dominant wetland type. Wetlands are typically shallow and do not

Table 1
Summary of key papers related to this study's research objectives (the current paper is added for completeness). In the 'key details' column the codes relate to the following criteria: (1.) Spatial resolution of surface water measurement (2.) Scale used for tracking change: wetland, pixel or landscape (3.) Temporal resolution: seasonal or long-term (4.) Application.

Study	Study area	Data used	# of image dates/time span	Method	Key details
1. Gómez-Rodríguez et al. (2010)	Doñana National Park, Spain	Landsat TM	174 dates 1984–2007	Developed a linear model using reflectance of near IR band to predict subpixel fractions of water cover.	1.) <30 m 2.) Pixel 3.) Seasonal and long-term 4.) Classified wetland types by hydroperiod and monitored wetland change over time.
2. Beeri & Phillips (2007)	Missouri Couteau, USA	Landsat TM	31 dates 1997–2005	Developed a regression model to identify surface water for waterbodies greater than a half a Landsat pixel.	1.) <30 m 2.) Pixel and landscape 3.) Seasonal and long-term 4.) Identified shifts in the distribution of hydroperiod classes within and between years
3. Huang et al. (2011)	Cottonwood Lake, North Dakota, USA	Landsat TM, aerial photos, lidar	26 (Landsat TM), 11 (aerial photos), 1 (lidar)	Developed a complex regression model using Landsat, Palmer Drought Severity Index, and aerial imagery to model surface water for wetlands as small as 0.8 ha.	1.) <30 m 2.) Wetland and landscape 3.) Seasonal and long-term 4.) Tracked changes to surface water from modeled result, which is driven by PDSI.
4. Huang et al. (2014)	Chesapeake Bay watershed, USA	Landsat TM, lidar intensity	4 dates 2005–2010	Developed a regression model using multiple variables including tasseled cap indices, NDVI, NDWI and Modified NDWI, and an infrared-visible ratio index to predict sub-pixel wetland inundation maps.	1.) <30 m 2.) Landscape 3.) N/A 4.) Tracked changes in inundation for a wet, dry, and average year and summarized at the landscape scale.
5. Reschke & Hüttich (2014)	Western Turkey	Landsat TM	3 dates 2002–2003	Mapped sub-pixel fractional wetland type (including water) using a Random Forest algorithm	1.) <30 m 2.) Pixel 3.) Seasonal 4.) Classified wetlands by type (i.e. marsh, mudflat, river, water), but not by hydroperiod
6. Collins et al. (2014)	Prairie Potholes, USA	Landsat TM	35 dates 2008–2011	Used a band ratio (bands 5, 3) to classify pixels as water, non-water.	1.) 30 m 2.) Pixel, wetland, landscape 3.) Seasonal and long-term 4.) Measured hydroperiod length of playa wetlands for 3 years and compared it to surrounding land use.
7. Frohn et al. (2012)	Ohio, USA	Landsat TM	2 dates 2002–2003	Developed a spectral mixture analysis partial unmixing model to detect sub-pixel inundation levels.	1.) <30 m 2.) Pixel 3.) N/A 4.) Identified isolated wetlands as small as 1/2 Landsat pixel.
8. Rover et al. (2010a)	Alaska, USA	Landsat TM, SPOT-5	One date N/A	Developed a self-trained regression tree using single band and multi band indices to map sub-pixel percent-water maps and compared results to other sub-pixel methods.	1.) <30 m 2.) Pixel 3.) N/A 4.) N/A
9. Niemuth, Wangler, & Reynolds (2010)	Prairie Pothole Region, USA	Aerial photos	20 dates 1987–2006	Used a combination of supervised classification and photo interpretation to map surface water area within wetlands.	1.) <8 m 2.) Wetland 3.) Long-term 4.) Examined spatiotemporal patterns of wetland inundation.
10. Our method	Douglas Co, WA, USA	Landsat TM Aerial photo	230 dates 1984–2011	Developed a 4 endmember spectral mixture analysis model to measure sub-pixel wetland inundation.	1.) <30 m 2.) Wetland 3.) Seasonal and long-term 4.) Classified wetland types by hydroperiod and monitored wetland change over time.

support floating vegetation. Wetland vegetation is restricted to areas that are seasonally flooded, often forming a ring around wetlands that are semi-permanently or permanently flooded. Refill of wetlands in this area is driven by snowmelt occurring in late winter or early spring. As the summer season progresses temperatures increase and precipitation levels decline. Wetlands begin to dry out during this time, and many are completely dry by the end of the summer. Short-term rainfall events are usually localized in nature and occur sporadically during the spring and summer months. Although the direct causes of hydrologic change are not clear due to lack of research, wetlands in the Columbia Plateau generally are known to be stressed from impacts caused by farming, grazing, and reduced groundwater levels.

3. Materials

3.1. Aerial imagery

We used two digital ortho-imagery (2006 and 2011) with 1-m pixel resolution freely available through the National Agricultural Inventory Program (NAIP) rectified to true ground +/− 6 m (Table 2). The 2006

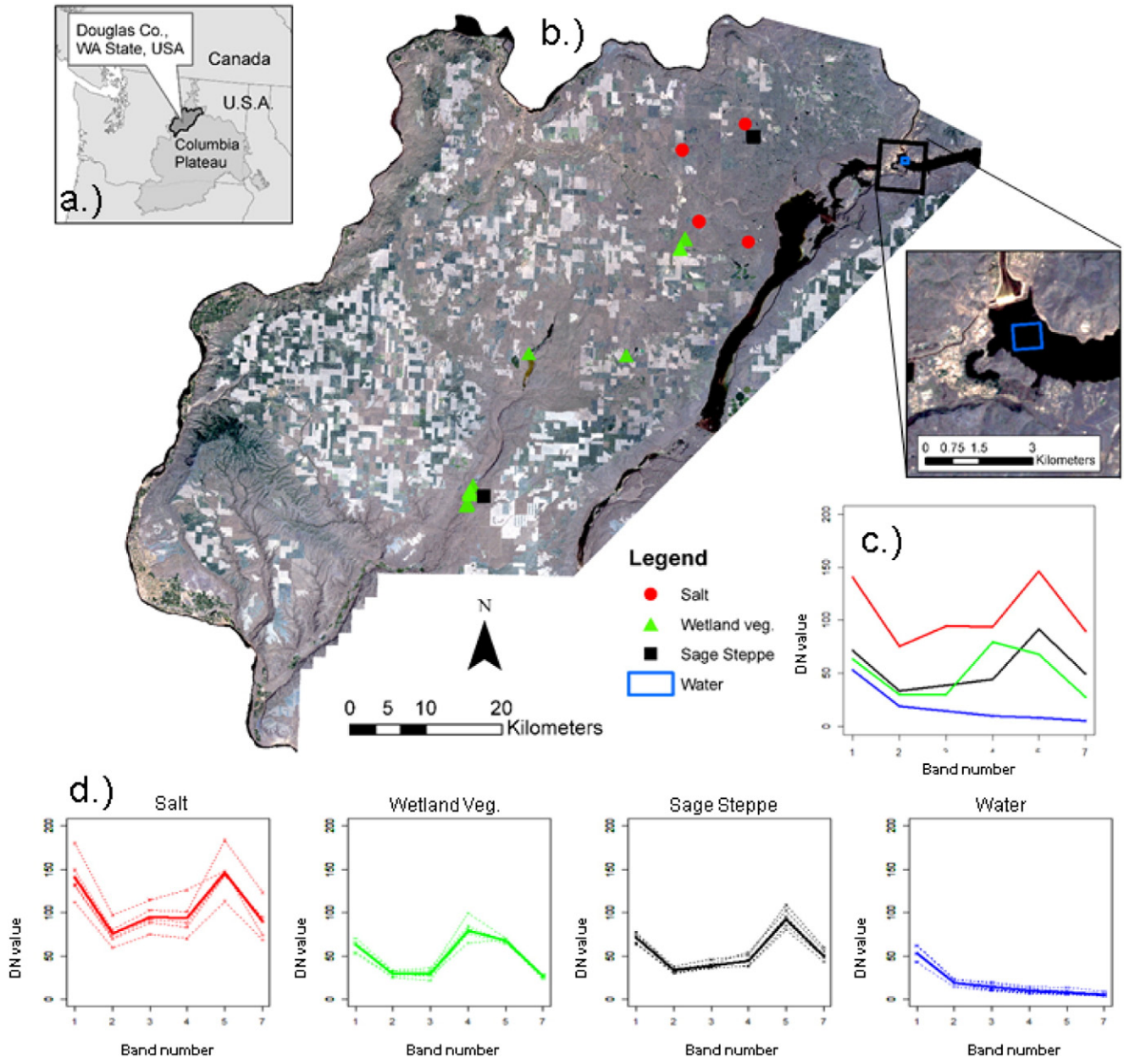

Fig. 1. a.) Study area, Douglas County, Washington state, USA. b.) Endmember locations. The background image is a Landsat TM 5 scene acquired on 07 Jul. 2011 and was clipped to our study area. c.)The graph represents the four endmembers used; water (blue), salt (orange), wetland vegetation (green), sage steppe (black). d.) Endmember graphs for salt and wetland vegetation from selected dates spanning the 1984–2011 timeframe used to derive a mean spectral signature for SMA. The graphs for sage steppe and water represent the image endmembers from the same date selection and illustrate the spectral variability across multiple image dates, but were not used for SMA. Instead, endmembers for water and sage steppe were selected directly from each image scene in the Landsat time series.

digital aerial image was a 3-band image (red, green, blue) and was acquired early in the summer of 2006 (exact date unknown), a wet year, when wetland water levels were high (USDA-FSA Aerial Photography Field Office, 2006). The 2011 aerial imagery was a 4-band image (NIR, red, green, blue) and was acquired between 06 Jul 2011 and 07 Jul 2011 (USDA-FSA Aerial Photography Field Office, 2011).

3.2. Landsat satellite imagery

We downloaded 230 Landsat Thematic Mapper 5 satellite images acquired between 1984 and 2011 from the United States Geologic Services GLOVIS website (http://glovis.usgs.gov/) using the batch download tool for our time series analysis. Our study area fell on two Landsat scenes, path 45 row 27 and path 44 row 27. Each image was visually assessed for quality, and only cloud-free images were chosen. All downloaded images were processed as Level 1 T terrain-corrected products. Because most wetlands in our study area freeze in the winter months and may be covered in snow, only snow-free images acquired between April 1 and October 30th were selected (Table 2).

4. Methods

We identified wetlands in our study area using an object-based image analysis classification of high-spatial-resolution aerial photography (Sections 4.1). For each identified wetland, we estimated the subpixel surface water area (m^2) from a four-endmember spectral mixture analysis (SMA) of Landsat TM imagery (Sections 4.2.1, 4.2.2). We then validated the SMA model for 750 wetlands by comparing surface water area from one Landsat image to wetland surface water area delineated from a matching date of high resolution aerial imagery

Table 2
Materials.

Datasets	Spatial resolution	Temporal resolution	Source
2006 digital aerial imagery	1 m	1–3 years	United States Department of Agriculture, National Agriculture Inventory Program
2011 digital aerial imagery	1 m	1–3 years	United States Department of Agriculture, National Agriculture Inventory Program
Landsat TM 5	30 m	16 days	United States Geological Survey http://glovis.usgs.gov/

(Section 4.2.3). Next, we reconstructed surface water hydrographs for all wetlands using the time-series of Landsat imagery from 1984 to 2011 (Section 4.3). Finally, we explored the dataset to determine if it could be used as a tool to classify wetlands by their hydrologic regime and monitor wetlands (Section 4.3). Fig. 2 provides a flowchart of these steps.

4.1. Data pre-processing

We used a high-resolution wetland classification for Douglas County to summarize spectral mixture results for individual wetlands. The wetland classification was created using object-based image analysis of 2006 digital aerial images with 1-m pixel resolution, freely available through the United States Department of Agriculture, National Agriculture Inventory Program (NAIP). The classification was created through a rule based algorithm using wetland features, such as color, shape and texture determined from manual photo interpretation and is described in Halabisky et al. (2011). The classification had an overall accuracy of 89% and a minimum mapping unit of 200 m^2.

We updated the wetland classification created from 2006 aerial imagery to classify wetlands that were dry or had been plowed since that time by adding the NAIP imagery from 2011 to the object based image analysis algorithm. In addition, we manually edited the updated classification to correct and remove misclassified wetland polygons (~40 h). Most misclassification errors were due to small shadows, rock outcrops, or road sections that were dark in color and were spectrally similar to water. With the additional date of imagery our accuracy minimally improved by 1% to an overall accuracy of 90.3% ($k = 0.85$) (Table 3). The confusion matrix was created using a stratified random sample of 177 points within the wetland classification and 100 additional points in the background matrix.

All wetland components (i.e. emergent vegetation, open water) were merged to form wetland complexes. Wetland complexes that consisted only of wetland vegetation were not used for this analysis. From this classification, we selected wetlands larger than 600 m^2. We buffered complexes by 30 m to allow for small spatial shifts between Landsat image scenes.

4.2. Objective 1: develop a method with minimal pre-processing to estimate surface-water extent for wetlands at scales below 30 m

4.2.1. Spectral mixture analysis

Spectral mixture analysis (SMA) is a method used to identify the fractional abundance of distinctive spectra, known as spectral endmembers, within the spectrum of a mixed pixel (Adams et al., 1986; Adams & Gillespie, 2006). Spectral endmembers represent samples of significant physical scene components and are selected from spectral measurements on the ground, spectral libraries ("reference" endmembers) or from the image itself ("image" endmembers). Samples measured on the ground generally are themselves mixtures and therefore do not yield "pure" spectral signatures of the material they represent. However, at image scales the spectral heterogeneity is commonly reduced and well-chosen spectra are sufficient for SMA (Adams & Gillespie, 2006). SMA has been shown to work well in water environments and in areas where there is high spectral contrast between classes (Shanmugam et al., 2006).

Mathematically, SMA can be expressed as:

$$DN_i = \sum_j F_j DN_{i,j} + r_i \text{ and } \sum_j F_j = 1 \quad (1)$$

where DN_i is the measured value of a mixed pixel in band i; DN_j is the measured value of each endmember; F_j is the fraction of each endmember; r is the root mean square (rms) residual that accounts for the difference between the observed and modeled values (Adams & Gillespie, 2006).

We developed our SMA model using ENVI software version 4.8 (Exelis Visual Information Solutions, Boulder, Colorado). For every Landsat image we used all bands, except band 6, the thermal infrared

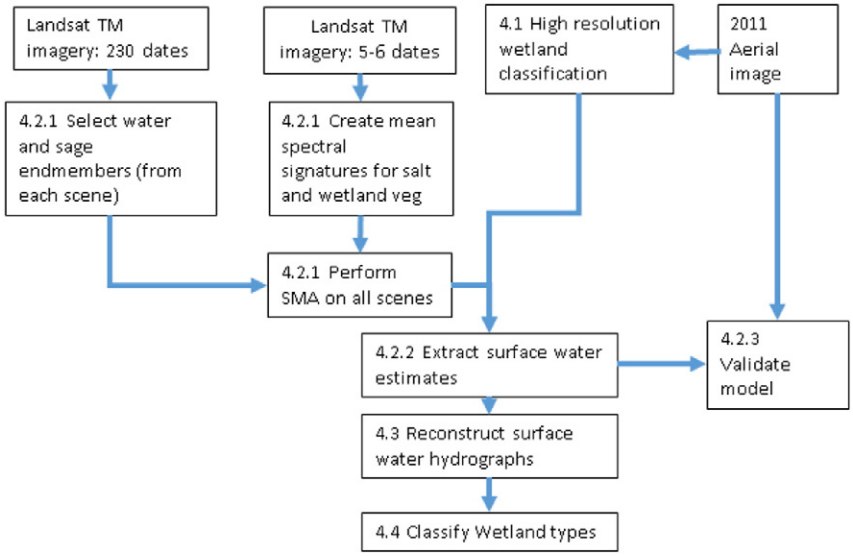

Fig. 2. Flowchart of method steps.

Table 3
Accuracy assessment for wetland classification with OBIA and NAIP imagery (overall accuracy = 90.3%, $k = 0.85$) in Douglas County, WA, 2011).

Reference data					
Classification data	Open water	Emergent vegetation	Background	Total	User's accuracy
Open water	68			68	100.0%
Emergent vegetation	4	82		86	95.3%
Background		23	100	123	81.3%
Total	72	105	100	277	
Producer's accuracy	94.4%	78.1%	100.0%		
Overall accuracy	90.3%				
k	0.85				

band. The image endmembers were selected from areas mapped as water, sage steppe, salt, and wetland vegetation. Salt was chosen because many of the wetlands form a salt crust when dry. Image endmembers for water and sage steppe were selected using specific geographic coordinates determined in the field based on our knowledge of the landscape and selected directly from each Landsat image (Fig. 1). The benefits of selecting an endmember from the image is that atmospheric correction is not required as long as the geographic extent is not too broad to have significant variation in atmospheric effects (Aspinall, Marcus, & Boardman, 2002). The water endmember was selected from a deep portion of the Columbia River behind the Grand Coulee Dam (Fig. 1). This part of the Columbia River has little to no flow and is low in suspended sediment therefore represents a reliable signature for water that remains stable throughout the year.

Spectrally pure pixels for salt and wetland vegetation are not apparent in every image. Therefore, we estimated image endmembers for salt and wetland vegetation using the mean spectral signature derived from an early summer and late summer image for three years: 1984, 1994, & 2004. Six images in total were used to calculate the mean endmember values for each of the six bands (29 Aug 1984, 28 Sep 1984, 24 Jul 1994, 26 Sep 1994, 30 May 1994, 30 Mar 2004, 21 Sep 2004) (Fig. 1). The 29 Aug 1984 endmember for salt was omitted because there was not a spectrally "pure" pixel for that scene. Therefore, the salt endmember was sampled from five images instead of six.

We performed no atmospheric correction because we selected our water endmember directly from each image in the time series, minimizing error in the endmember fractions caused by atmosphere. However, because we used average spectra for two of our endmembers we cannot completely remove error from endmember fractions caused from changes in atmosphere between image dates. A sum-constrained linear spectral mixture model (for ENVI, an arbitrary but large sum constraint = 10,000 was specified, corresponding to the endmember fraction summing to ~1.00) was run on all scenes. Only the fractional abundances for water and the root mean square (rms) error were exported as a two-band image. Proportion of surface water generally ranged from <0 to 1.0, with some surface water values above 1.0. Any score below zero represents pixels with no surface water, while scores of 1.0 or above represent pixels composed entirely of surface water. We ran our SMA model on all 230 Landsat image scenes using batch processing in ENVI IDL (Exelis Visual Information Solutions, Boulder, Colorado). Total processing time took roughly 4 h.

4.2.2. Estimating surface water extent for wetlands

In order to estimate the surface water extent for wetlands we first converted all pixels from the SMA output to sub-pixel surface water area estimates (m^2). To do this we multiplied the fractional abundance of surface water for each pixel by the area of the pixel (i.e. 900 m^2). This provided a sub-pixel surface water area estimate for each pixel in the image scene (Fig. 3).

Next, we summarized the sub-pixel surface water area estimates for each wetland using the buffered high-resolution wetland classification derived from 2006 and 2011 aerial imagery. The buffered wetland polygons were used to select (known as "extract by polygon" in ArcGIS) corresponding sub-pixel surface water area estimates which were summed for each wetland using python tools in ArcGIS 10.1 (ESRI, Redland, California). Mathematically this can be expressed as:

$$\sum_{i=1}^{n} F_i * a \tag{2}$$

where F is the fractional abundance of water for pixel i; a is the area of one Landsat pixel (i.e. 900 m^2) and n is the number of pixels selected for each wetland polygon.

4.2.3. Validation

We used the 07 Jul 2011 Landsat image to validate our four-endmember SMA model. We compared SMA wetland surface water extent for this image to a reference dataset created through manual delineation of wetlands using high-resolution aerial imagery acquired at the same time (06 Jul 2011–07 Jul 2011). To build our reference dataset, we used sampling with probability proportional to size to select 100 wetland polygons from our wetland classification. We chose this sampling strategy for two reasons. First, we did not set a minimum mapping unit and wanted to see how error changed across multiple wetland sizes. Second, because wetlands <1 ha dominate the landscape an entirely randomly sample of wetland polygons would result in a sample primarily consisting of very small wetlands. The surface water extent of wetlands in the validation dataset ranged from 0 (completely dry) to 22.48 ha.

In order to understand error in terms of percent change we converted surface water area estimates into percentages by relativizing surface water area by the maximum inundation extent (derived from Landsat) for each wetland. We also relativized the reference dataset by the maximum inundation and compared it to the percent surface water from the SMA. We plotted the residuals from the relationship between percent actual surface water extent and percent modeled surface water extent against wetland size to see if error changed across wetland size.

We assessed the rms output for the 07 Jul 2011 Landsat satellite image scene to determine that the four endmember SMA model accounted for all surface materials within each wetland polygon and calculated the percentage of pixels with a rms error above 2 DNs. Additionally, we calculated the mean rms error for an area in the Columbia River that represented a homogenous body of water with the assumption that a model with acceptable levels of noise should have DN values below 2 (Nichol & Vohora, 2004).

4.3. Objective 2: reconstruct hydrographs

Surface water area estimates from all images (1984–2011) were exported for each wetland and used to reconstruct individual surface-water hydrographs using plotting tools in R statistical software (R Core Team, 2013).

4.3.1. Validation

No formal validation was performed on the reconstructed hydrographs, because we could find only one high-resolution aerial image acquired at the same time as a Landsat image. Instead, we visually compared hydrographs to annual precipitation patterns for the same time period (1984–2011). Monthly precipitation totals came from the PRISM Climate Group, Oregon State University, http://prism.oregonstate.edu (created 4 May 2015), which gathers climate observations from a wide range of monitoring networks and develops spatial climate datasets covering the conterminous United States (Daly et al., 2008). We plotted a moving average of annual precipitation using monthly precipitation totals as taken from PRISM data along with our

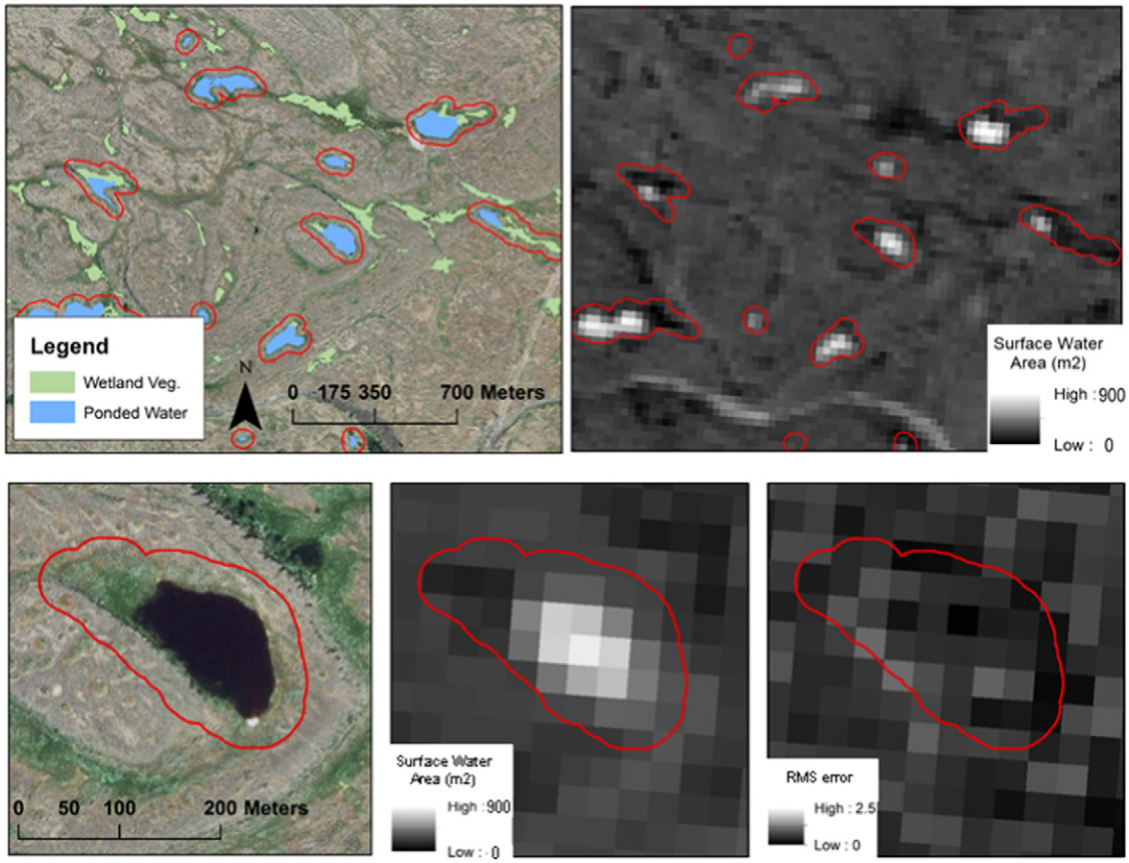

Fig. 3. Example of combining high-resolution classification and sub-pixel surface water estimates from SMA. Wetland complexes, including pond and wetland vegetation (top left) were buffered by 30 m (red outlines). SMA results (top right) were summed for each wetland polygon to derive surface water extent. The example on the bottoms shows from left to right, a buffered wetland, the SMA results converted to surface water area, and rms error for one wetland, 3.4 ha in size.

reconstructed hydrograph to visually assess if wetland surface water area generally tracked changes in precipitation.

4.4. Objective 3: use hydrographs to classify wetland types and monitor wetland change over time

The methods above enabled us to reconstruct wetland hydrographs. We then explored these reconstructed hydrographs to determine if the dataset could be used as a tool to classify and monitor wetlands. We classified wetlands in two ways. First, we categorized wetlands based on the percentage of years a wetland dried out. We considered a wetland dry when surface water extent fell below a threshold of 25% as not all years captured the exact date of 100% drying. Because the wetlands in Douglas County are shallow, depressional wetlands when the surface area of water in a wetland falls below 25%, the water depth is very shallow and the wetland is near drying. Next, we classified wetlands by hydroperiod type based on the seasonal patterns of an average year of precipitation (2011) using wetland hydrologic modifiers from the Cowardin classification scheme; temporarily flooded, seasonally flooded, and permanently flooded (Cowardin, Carter, Golet, & Laroe, 1979). Temporarily flooded wetlands only hold water for brief periods in the growing season. Seasonally flooded wetlands hold water for extended periods in the growing season, but are usually completely dry by early summer. A permanently flooded wetland shows little change in surface water area throughout the summer months.

In order to determine if hydrographs could be used to monitor wetland change we selected all wetlands with maximum surface water extent above 1 ha as patterns are more distinct at this scale to create a subset of 481 wetland hydrographs. We next, organized hydrographs with similar patterns into unique groups. We looked at historic imagery of a sample of wetlands from each group to determine if we could distinguish the cause of the hydrograph pattern.

5. Results

5.1. Objective 1: develop a method with minimal pre-processing to estimate surface-water extent for wetlands at scales below 30 m

Our method captured the surface water extent for each wetland within our wetland classification for our 07 Jul 2011 Landsat image. The rms image had no distinct pattern within the wetland boundaries (Fig. 3), indicating that the SMA technique accounted for all significant endmembers. Because the objective was to estimate surface water extent, we were not concerned about error rates outside of the delineated wetland basins. Twenty percent of pixels within the wetland classification had an rms error above 2 DNs. Sampling of pixels behind Grand Coulee Dam on the Columbia River, a homogenous waterbody, had a low rms error. Mean rms error was 0.45 DNs with all rms error for the Columbia River falling within a range of image noise between 0.06 and 1.14 DNs.

Comparisons of the SMA wetland surface water estimates to the validation dataset show a R^2 value of 0.99 ($p < 0.001$) (Fig. 4) and a standard error of 0.85. Percent surface water estimates, as expected, had a lower correlation, with a R^2 value 0.85 ($p < 0.001$) (Fig. 4) and a standard error of 0.08. Although, still low, further examination of the residuals compared to the size of the wetlands shows a larger magnitude of error for smaller wetlands (Fig. 5)

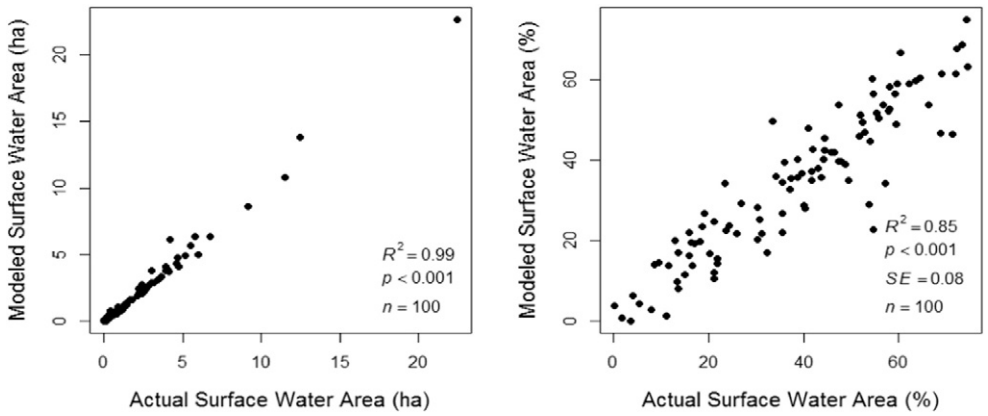

Fig. 4. Figure on left shows the comparison of modeled surface water area as derived from SMA method against actual surface water area derived from manual delineation of aerial photos. Figure on right shows the percent of modeled surface water extent compared to the percent of the actual surface water extent. Percent surface water extent was derived by relativizing wetland surface water area by the maximum flooded area derived from SMA time series.

5.2. Objective 2: reconstruct individual wetland hydrographs from 1984 to 2011

Our technique produced detailed hydrographs for 750 wetlands spanning a time period from 1984 to 2011, across Douglas County. The individual hydrographs capture both long-term change and seasonal change to surface water extent within wetlands and appear to follow changes in precipitation levels (Fig. 6). As described above smaller wetlands had higher error. An example of a small wetland hydrograph is shown in Fig. 7. This wetland has a maximum size of 1530 m^2. The validation dataset estimated the surface water extent for this wetland (derived from the 2011 aerial image) to be only 800 m^2 in size, less than one Landsat pixel. The SMA technique estimated the wetland to be 140 m^2. Of all the wetlands in the validation dataset it has the highest residual (28%). Despite this error it is clear that this wetland only fills up during wet years (mid 1980s, mid 1990s, and a few years in the 2000s), when precipitation levels are above average.

5.3. Objective 3: use hydrographs to classify wetland types and monitor wetland change over time

Reconstructed hydrographs show seasonal change and can be used for classification of wetland by hydroperiod type. Fig. 8 shows the hydrograph for three different wetland hydroperiod types based on both long-term and seasonal patterns found within the dataset. Note, that although the three wetlands (Fig. 8 a, b &c) are different sizes, they are distinguished by their hydrologic regime not their size. A temporarily flooded wetland (Fig. 8a) dries up early in the summer season in an average year of precipitation and dries up most years. A seasonally flooded wetland (Fig. 8b) dries up between 51 to 75% of the years that we measured. In an average year of precipitation it significantly declines in surface area, but does not completely dry up. A permanently flooded wetland (Fig. 8c) does not dry up and has little seasonal change to surface water extent.

We detected five different patterns of wetland hydrographs. The first group (318 wetlands), appeared to follow precipitation patterns similar to the patterns evident in Figs. 6–8. The second group of hydrographs (42 wetlands) did not track precipitation levels and had an irregular zigzag pattern (Fig. 9). These hydrographs represent misclassification error carried over from the wetland classification. This hydroperiod pattern is likely due to shadows that were misclassified as open water wetlands in the wetland classification. The hydrograph for the misclassified shadow appears to increase in surface water extent during summer for three years (1984, 1993, 2011), which is likely driven by seasonal changes in the cast shadow as there is no wetland evident in the aerial photo.

The remaining wetland hydrographs diverged from long-term precipitation patterns (Fig. 10), but did not have the same regular zigzag pattern as those in the second group. The third group (84 wetlands) showed an obvious decrease in surface water extent over time. Fig. 10 (top) provides an example of a wetland that is drying out over time and is now has only 50% of the total surface water extent it had in the mid-1980s. The fourth group (32 wetlands) show irregular patterns of flooding and drying. Fig. 10 (middle) is an example of a wetland that is repeatedly plowed over for farming. The fifth group (5 wetlands) is rare on this landscape, but shows an increase in long-term surface water extent. Fig. 10 (bottom) shows a hydrograph of a wetland that was created through hydrologic engineering.

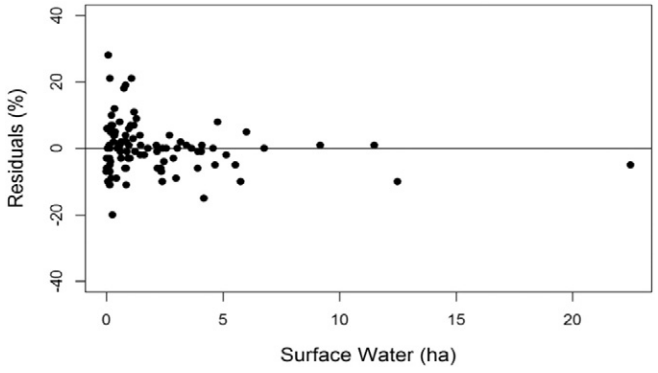

Fig. 5. Residuals of relationship between percent predicted surface-water extent to percent actual surface water extent. Surface water extent as measured by the validation dataset is plotted on the x-axis.

6. Discussion

Our method provided detailed hydrological data for all surface water wetlands within our 4714 km^2 study area of Douglas County, WA, USA with minimal data pre-processing. The individual hydrographs capture both long-term and seasonal change to surface water extent of wetlands. To the best of our knowledge, this is the first such reconstruction of wetland hydrographs for all wetlands across a broad landscape at such a fine spatial and temporal resolution. As such, it offers novel insight into landscape-level wetland dynamics, reconstructs data for testing hydrologic or ecological hypotheses, and provides a useful tool for hydrological monitoring of wetlands at multiple scales; from large landscape analysis to individual wetland monitoring in high contrast semi-arid locations in the western United States.

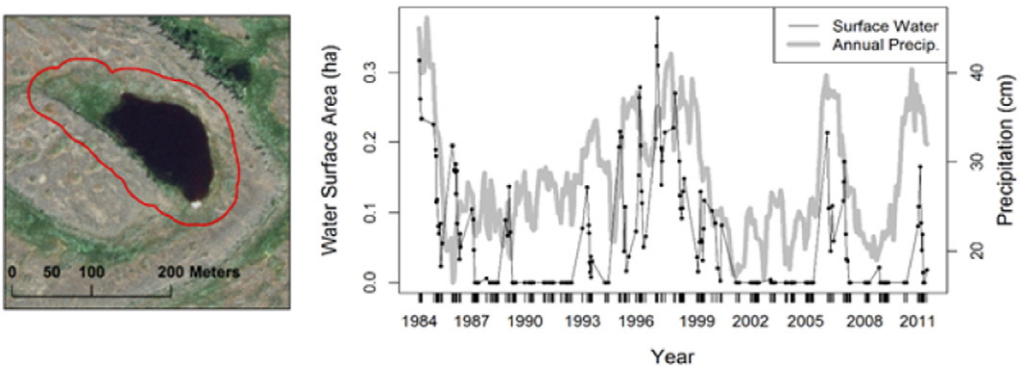

Fig. 6. Example of a hydrograph spanning 1984–2011. This figure represents the hydrograph of the wetland highlighted in Fig. 3, which is 3.4 ha in size. X-axis tick marks represent number of observations. Reconstructed hydrograph measures both inter- and intra- annual change. A moving average of annual precipitation calculated from monthly totals is shown in gray. The hydrograph of this wetland appears to follow changes in precipitation levels.

6.1. Sources of error

Spectral mixture analysis yields spectral abundance of the spectral endmembers in the mixed pixel spectrum. It is related to the physical abundance of the corresponding physical endmember, but is not necessarily a one-to-one ratio. A likely source of error is due to a mismatch between the image endmember chosen in our SMA model, which came from deep water, and water contained in wetlands. The spectral endmember we chose for water was likely closely matched to the physical endmember we modeled except where algae, floating vegetation, and areas of shallow water, occurred in wetlands. Wetlands containing wet mud may look partially filled with water because of spectral mixing between water and mud. In addition, we cannot completely remove atmospheric error from endmember fractions because we used average spectra for two of our endmembers.

As indicated in Fig. 5, error was greatest for small wetlands. Smaller wetlands are composed of fewer Landsat pixels and more likely to be composed of mixed pixels. Because our model used average spectra for two of endmembers (i.e. salt and wetland vegetation) we assume that error will be greatest for small wetlands which are composed of mixed pixels that contain proportions of these two endmembers. Although the accuracy decreased for smaller wetlands, it still provides useful information on their hydrology and could be used even on wetlands smaller than two Landsat pixels (1800 m^2) for monitoring of large disturbance to wetland hydrology (e.g. land conversion). Despite higher levels of error, this method still provides useful information on the hydrology of very small wetlands (Fig. 7).

Our validation method does not assess error outside of our wetland classification. Therefore, it is important to use a wetland classification that accurately delineates wetlands and has both low errors of commission and low errors of omission. Although a high-resolution wetland inventory exists for our study area (i.e. the US National Wetland Inventory), it did not meet this criteria. Ideally, we would have preferred a classification derived from historical aerial imagery acquired prior to 1984 so that we could capture wetlands that had been filled or drained before 2006, the date of imagery that our classification is based on.

6.2. Method strengths and limitations

Rather than tracking surface water extent of individual pixels through time or summarizing changes to surface water at the landscape scale as in previous approaches, our method reconstructs hydrographs specifically for individual wetlands. Because of this, our SMA model measures surface water extent in terms of area, providing an intuitive dataset. By contrast, it can be difficult to understand how other subpixel methods based on remote-sensing indices or changes in band reflectance (e.g. Landsat TM 5 Band 5) translate to on-the-ground conditions without field calibration. However, our method measures surface water extent, not water depth which is of great utility in wetland science. Additional research would be necessary to determine if surface water area could be converted into water depth or water volume. The addition of a high resolution digital terrain models derived from infrared lidar flown when wetlands are dry or the use of green lidar to

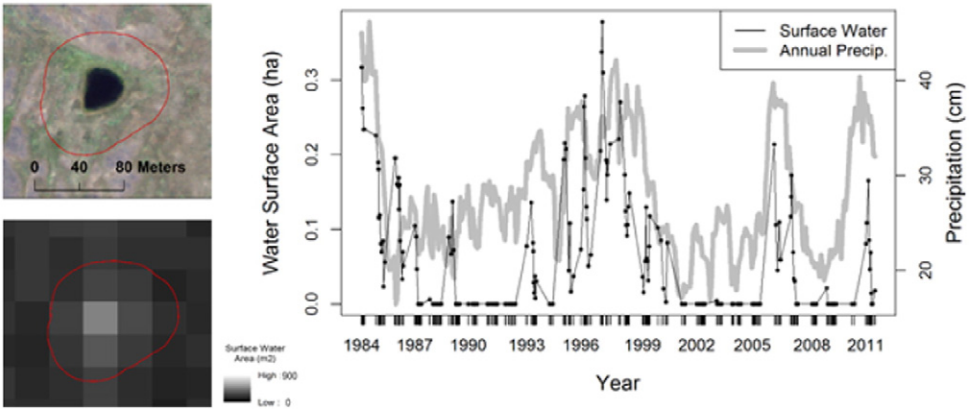

Fig. 7. Example of a hydrograph for a small wetland. This wetland had a maximum size of 1530 m^2. The surface area of the validation dataset (derived from 2011 aerial image) estimated the surface area to be only 845 m^2 in size (less than one Landsat pixel).

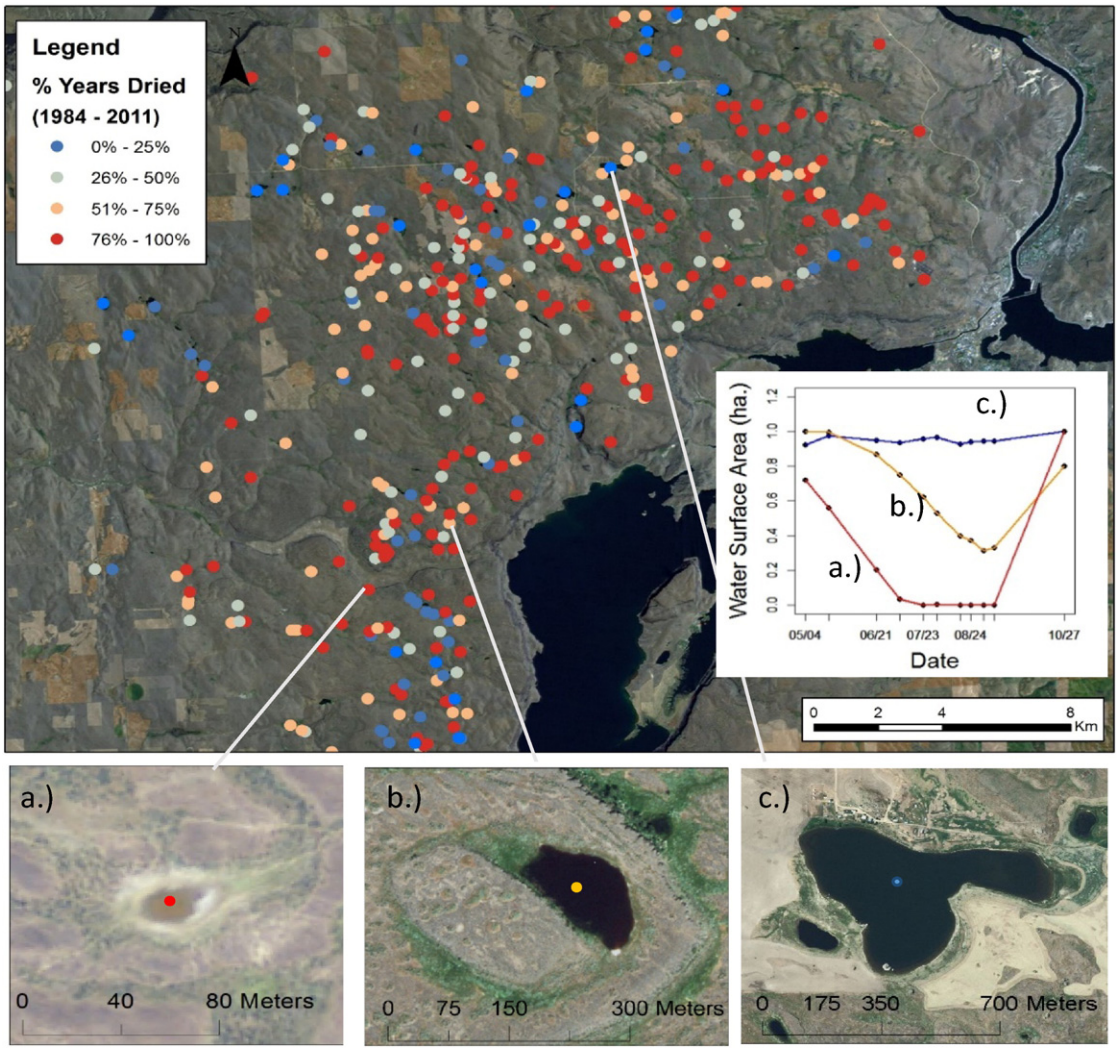

Fig. 8. Example of a hydrograph for three different wetland types for the year 2011; temporarily flooded wetland (a.), seasonally flooded wetland (b.), and a permanently flooded wetland (c.). The map shows the spatial variability of wetland types in northeast Douglas County based on the number of years the wetland fell below 25% water surface area between 1984 and 2011.

map wetland bathymetry may prove fruitful (Allouis, Bailly, Pastol, & Le Roux, 2010; Lane & D'Amico, 2010; Richardson & Moskal, 2014).

Because our method incorporates a high-resolution wetland delineation it works best for discrete wetlands that can be delineated into polygons. For extensive and complex wetlands it may not be useful to track surface water extent of the entire wetland. In these instances it could be more useful to track individual pixels through time using other methods such as those outlined by Gómez-Rodríguez et al. (2010).

An additional limitation is that accurate wetland classifications are not available in many areas. However, it is important to note that in some instances manual delineation of wetlands may provide an adequate alternative to remotely sensed classifications. Furthermore, our method can be used as a tool to automate removal of erroneously classified shadows from a dataset because as demonstrated in Fig. 9 shadows have a unique temporal signature.

Areas with limited high-quality cloud-free Landsat imagery may not benefit from this method because the imagery may be too infrequent to reconstruct meaningful hydrographs. Additionally, wetlands with short hydroperiods may not be captured at the interval of Landsat imagery (i.e. 16 days). In these instances, other methods that used multiple Landsat images to predict the hydrologic regime of wetlands (Beeri & Phillips, 2007; Reschke & Hüttich, 2014) may be more appropriate.

Our method requires selecting an image endmember from deep, sediment free water within the image scene. Accuracy would be impacted if the image endmember was not sampled from a spectrally pure water sample or included seasonal changes in water clarity either in the image endmember or in the wetlands themselves. This requirement cannot be met in many landscapes.

Douglas County has few trees, subtle topography, and therefore few resolved shadows. Further testing across more diverse and complex landscapes is necessary to determine applicability of our method in non-arid landscapes. As shadows and water have similar spectral signatures, this method would not work well in areas where shadows mixed with wetland area, such as forested wetlands or areas with steep topography. Without significant modification this method would not work on wetlands with little or no surface water, such as wet meadows.

6.3. Potential applications

Unlike rivers and streams, which are typically monitored in greater numbers and at higher frequencies, hydrologic data for wetlands is unavailable for the vast majority of regions. This limitation has inhibited exploration of questions related to wetland hydrology and advancement of basic scientific understanding of wetland dynamics for some time (Mitsch & Gosselink, 2007). Our method opens a new area of

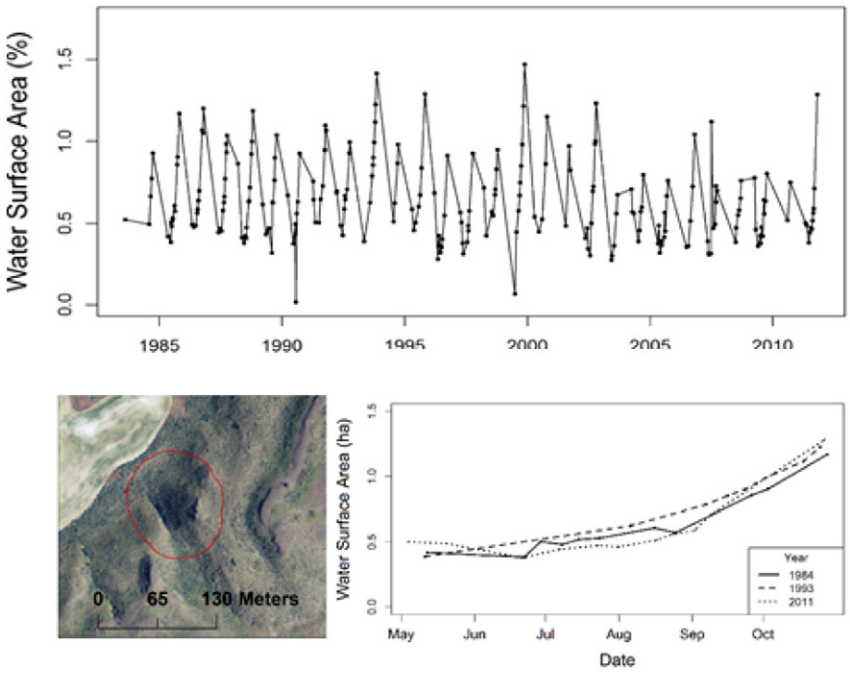

Fig. 9. Example of a 'hydrograph' of a shadow that was misclassified as a wetland. The long-term hydrograph (top) has a zig zag pattern that does not follow precipitation patterns. The lower right hand graph shows the seasonal hydrograph for three years (1984, 1993, & 2011). Surface water extent increases through the summer season, contrasted with a typical wetland which dries out as the summer temperatures increase and precipitation levels typically decrease.

wetland science by potentially providing rich hydrologic data for a large number of wetlands over a broad landscape.

By providing a large sample size of wetland data covering a broad area, our method facilitates myriad explorations including characterizing wetlands and classifying wetland habitat types (Snodgrass, Komoroski, Bryan, & Burger, 2000), understanding environmental variability (LaBaugh, Winter, & Rosenberry, 1998), evaluating the relationships between wetland dynamics and climate variables (Winter, 2000), calibrating hydrologic models of climate impacts (Lee et al., 2015), quantifying ecosystem services (Woodward & Wui, 2001), and

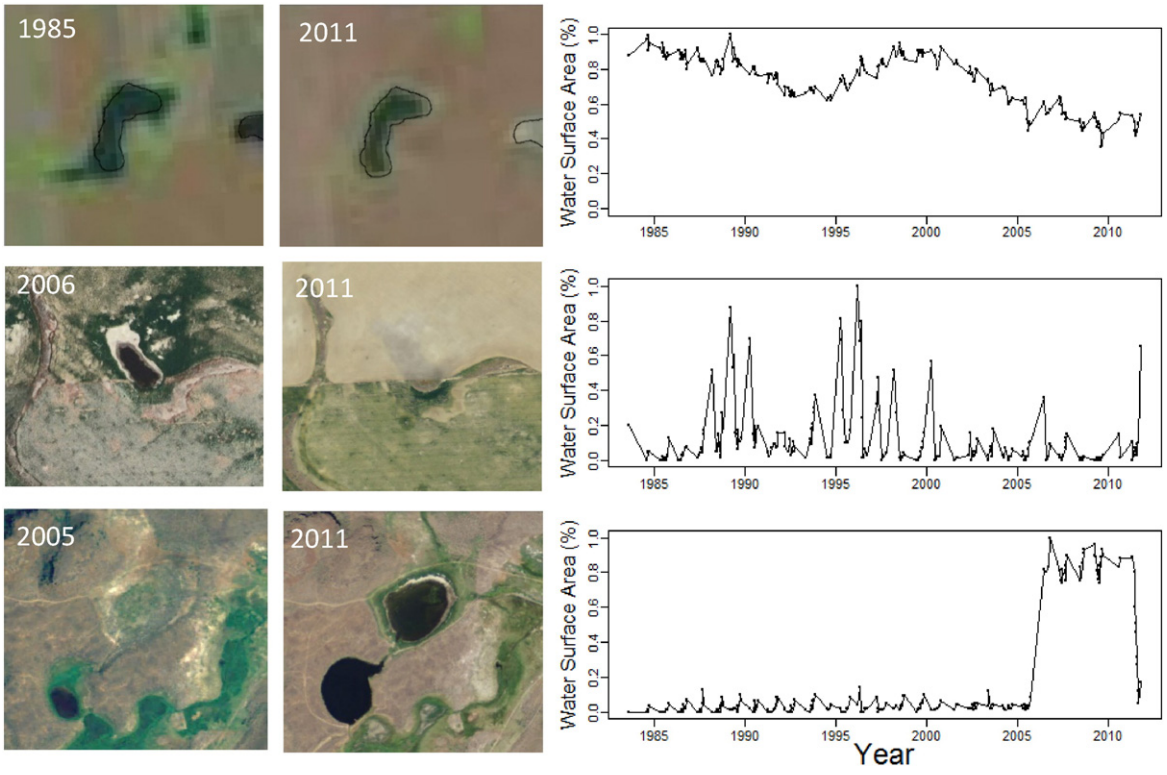

Fig. 10. Example of hydrographs for three wetlands undergoing abnormal change; shrinking wetland (top), plowed wetland (middle), and created wetland (bottom).

elucidating the role of groundwater or other hydrologic inputs. When coupled with biological data, these data support novel ecological investigations that have been hindered by the lack of time series data for wetlands. Opportunities include basic research on the relationship between hydrologic variation and species occupancy, composition, and richness (Tavernini et al., 2005); population or community dynamics and species diversity maintenance (Boyce et al., 2006; Chesson, 2000; Morris et al., 2008; Tuljapurka, 1990); metapopulation and metacommunity dynamics (Hanski & Gaggiotti, 2004; Leibold et al., 2004) and ecosystem services (Brauman, Daily, Duarte, & Mooney, 2007). Reconstructed hydrologic data also greatly enhance capacity for applied research on endangered species or critical ecosystem responses to hydrologic variation. For example, time-series data can be used to establish baselines and evaluate trajectories of change and risk associated with shifts in land use and climate change. Comparing hydrographs with precipitation or land use change data via formal time series analysis would be another fruitful avenue that may elucidate causes of hydrologic variability in wetlands.

Additionally, our method can be used as a monitoring tool by identifying abnormal changes to wetland hydrology (Kentula, 2007) and assessment of regional trends over time, including shifts in the relative coverage of different wetland types and changes in wetland function critical to understanding the full picture of wetland dynamics beyond direct land conversion.

7. Conclusion

We demonstrated a reliable and cost-effective method for wetland assessment that provides information on status and trends of surface water for individual wetlands in semi-arid regions. Our approach using high-resolution wetland delineations and spectral mixture analysis of Landsat imagery substantially increases the available hydrologic data for wetlands by reconstructing detailed wetland hydrographs without the need for extensive pre-processing. These methods allow for new insights into landscape level changes to wetland hydrology and conservation actions. Further research is needed to test limitations in other non-arid regions.

Acknowledgments

This research was funded by the United States Geological Survey, Department of the Interior Northwest Climate Science Center (USGS grant #GS276A-AUSGS), and the University of Washington Precision Forestry Cooperative. The authors would like to thank Chris Vondrasek and Max Sugarman for their assistance with field work and manual photo interpretation of wetlands and Maureen Ryan and Aaron Johnston for their valuable feedback on this manuscript. Additionally, the authors would like to thank the anonymous reviewers and Associate Editor Tim McVicar for their helpful feedback on an earlier draft.

References

Adams, J.B., & Gillespie, A.G. (2006). Spectral-mixture analysis. *Remote Sensing of Landscapes With Spectral Mages; A Physical Modeling Approach* (pp. 126–165). Cambridge, UK: Cambridge University Press.

Adams, K.D., & Sada, D.W. (2014). Surface water hydrology and geomorphic characterization of a playa lake system: Implications for monitoring the effects of climate change. *Journal of Hydrology*, *510*, 92–102. http://dx.doi.org/10.1016/j.jhydrol.2013.12.018.

Adams, J.B., Smith, M.O., & Johnson, P.E. (1986). Spectral mixture modeling: A new analysis of rock and soil types at the Viking Lander 1 Site. *Journal of Geophysical Research - Solid Earth*, *91*(B8), 8098–8112. http://dx.doi.org/10.1029/JB091iB08p08098.

Allouis, T., Bailly, J.S., Pastol, Y., & Le Roux, C. (2010). Comparison of LiDAR waveform processing methods for very shallow water bathymetry using Raman, near-infrared and green signals. *Earth Surface Processes and Landforms*, *35*(6), 640–650. http://dx.doi.org/10.1002/esp.1959.

Arnell, N., Liu, C., Compagnucci, R., Cunha, L. da, Hanaki, K., Howe, C., ... Stakhiv, E. (2001). Hydrology and water resources: impacts, adaptation, and vulnerability : contribution of Working Group II to the third assessment report of the intergovernmental panel on climate change. *Climate Change*, *191–233*.

Aspinall, R.J., Marcus, W.A., & Boardman, J.W. (2002). Considerations in collecting, processing, and analysing high spatial resolution hyperspectral data for environmental investigations. *Journal of Geographical Systems*, *4*(1), 15–29. http://dx.doi.org/10.1007/s101090100071.

Babbitt, K.J. (2005). The relative importance of wetland size and hydroperiod for amphibians in southern New Hampshire, USA. *Wetlands Ecology and Management*, *13*(3), 269–279. http://dx.doi.org/10.1007/s11273-004-7521-x.

Beeri, O., & Phillips, R.L. (2007). Tracking palustrine water seasonal and annual variability in agricultural wetland landscapes using Landsat from 1997 to 2005. *Global Change Biology*, *13*(4), 897–912. http://dx.doi.org/10.1111/j.1365-2486.2006.01306.x.

Boyce, M.S., Haridas, C.V., Lee, C.T., Boggs, C.L., Bruna, E.M., Coulson, T., ... Tuljapurkar, S.D. (2006). Demography in an increasingly variable world. *Trends in Ecology & Evolution*, *21*(3), 141–148. http://dx.doi.org/10.1016/j.tree.2005.11.018.

Brauman, K.A., Daily, G.C., Duarte, T.K., & Mooney, H.A. (2007). The nature and value of ecosystem services: An overview highlighting hydrologic services. *Annual Review of Environment and Resources*, *32*(1), 67–98. http://dx.doi.org/10.1146/annurev.energy.32.031306.102758.

Bryant, R.G., & Rainey, M.P. (2002). Investigation of flood inundation on playas within the zone of chotts, using a time-series of AVHRR. *Remote Sensing of Environment*, *82*, 360–375. http://dx.doi.org/10.1016/S0034-4257(02)00053-6.

Castaneda, C., & Herrero, J. (2005). The water regime of the Monegros playa-lakes as established from ground and satellite data. *Journal of Hydrology*, *310*(1-4), 95–110 (Retrieved from <Go to ISI>://000230436200006).

Chesson, P. (2000). General theory of competitive coexistence in spatially-varying environments. *Theoretical Population Biology*, *58*(3), 211–237. http://dx.doi.org/10.1006/tpbi.2000.1486.

Collins, S.D., Heintzman, L.J., Starr, S.M., Wright, C.K., Henebry, G.M., & McIntyre, N.E. (2014). Hydrological dynamics of temporary wetlands in the southern Great Plains as a function of surrounding land use. *Journal of Arid Environments*, *109*, 6–14. http://dx.doi.org/10.1016/j.jaridenv.2014.05.006.

Correa-Araneda, F.J., Urrutia, J., Soto-Mora, Y., Figueroa, R., & Hauenstein, E. (2012). Effects of the hydroperiod on the vegetative and community structure of freshwater forested wetlands, Chile. *Journal of Freshwater Ecology*, *27*(3), 459–470. http://dx.doi.org/10.1080/02705060.2012.668719.

Cowardin, L.M., Carter, V., Golet, F.C., & Laroe, E.T. (1979). Classification of wetlands and deepwater habitats of the United States. *Wildlife Research*, *79* (doi: FWS/OBS-79/31, 2004 (December 1979)).

Dai, X. (1998). The effects of image misregistration on the accuracy of remotely sensed change detection. *IEEE Transactions on Geoscience and Remote Sensing*, *36*(5 PART 1), 1566–1577. http://dx.doi.org/10.1109/36.718860.

Daly, C., Halbleib, M., Smith, J.I., Gibson, W.P., Doggett, M.K., Taylor, G.H., ... Pasteris, P.P. (2008). Physiographically sensitive mapping of climatological temperature and precipitation across the conterminous United States. *International Journal of Climatology*, *28*(15), 2031–2064. http://dx.doi.org/10.1002/joc.1688.

Downing, J.A., Prairie, Y.T., Cole, J.J., Duarte, C.M., Tranvik, L.J., Strigel, R.G., ... Middelburg, J.J. (2014). The global abundance and size distribution of lakes, ponds, and impoundments. *Limnology and Oceanography*, *51*(5), 2388–2397. http://dx.doi.org/10.4319/lo.2006.51.5.2388.

Dyke, E., & Wasson, K. (2005). Historical ecology of a central California estuary: 150 years of habitat change. *Estuaries*, *28*(2), 173–189. http://dx.doi.org/10.1007/BF02732853.

Environmental Laboratory (1987). *Corps of engineers wetlands delineation manual, technical report Y-87-1*. Vicksburg, MS: U.S. Army Engineer Waterways Experiment Station.

Foody, G.M. (2000). Estimation of sub-pixel land cover composition in the presence of untrained classes. *Computers and Geosciences*, *26*(4), 469–478. http://dx.doi.org/10.1016/S0098-3004(99)00125-9.

Frohn, R.C., D'Amico, E., Lane, C., Autrey, B., Rhodus, J., & Liu, H. (2012). Multi-temporal sub-pixel Landsat ETM+ classification of isolated wetlands in Cuyahoga County, Ohio, USA. *Wetlands*, *32*(2), 289–299. http://dx.doi.org/10.1007/s13157-011-0254-8.

Gallant, A. (2015). The challenges of remote monitoring of wetlands. *Remote Sensing*, *7*(8), 10938–10950. http://dx.doi.org/10.3390/rs70810938.

Gilmer, D.S., Work, E.A., Colwell, J.E., & Rebel, D.L. (1980). Enumeration of prairie wetlands with Landsat and aircraft data. *Photogrammetric Engineering and Remote Sensing*, *46*(5), 631–634 (Retrieved from <Go to ISI>://A1980JS86200002).

Gómez-Rodríguez, C., Bustamante, J., & Díaz-Paniagua, C. (2010). Evidence of hydroperiod shortening in a preserved system of temporary ponds. *Remote Sensing*, *2*, 1439–1462. http://dx.doi.org/10.3390/rs2061439.

Halabisky, M., Moskal, L.M., & Hall, S.A. (2011). Object-based classification of semi-arid wetlands. *Journal of Applied Remote Sensing*, *5*, 053511. http://dx.doi.org/10.1117/1.3563569.

Hanski, I., & Gaggiotti, O. (2004). Metapopulation biology. Past, present, and future. *Ecology, genetics and evolution of metapopulations* (pp. 3–22). http://dx.doi.org/10.1016/B978-012323448-3/50003-9.

Huang, S., Dahal, D., Young, C., Chander, G., & Liu, S. (2011). Integration of Palmer drought severity index and remote sensing data to simulate wetland water surface from 1910 to 2009 in Cottonwood Lake area, North Dakota. *Remote Sensing of Environment*, *115*(12), 3377–3389. http://dx.doi.org/10.1016/j.rse.2011.08.002.

Huang, C., Peng, Y., Lang, M., Yeo, I. -Y., & McCarty, G. (2014). Wetland inundation mapping and change monitoring using Landsat and airborne LiDAR data. *Remote Sensing of Environment*, *141*, 231–242. http://dx.doi.org/10.1016/j.rse.2013.10.020.

Hui, F., Xu, B., Huang, H., Yu, Q., & Gong, P. (2008). Modelling spatial–temporal change of Poyang Lake using multitemporal Landsat imagery. *International Journal of Remote Sensing*, *29*, 5767–5784. http://dx.doi.org/10.1080/01431160802060912.

Kentula, M.E. (2007). Foreword: Monitoring wetlands at the watershed scale. *Wetlands*. http://dx.doi.org/10.1672/0277-5212(2007)27[412:FMWATW]2.0.CO;2.

LaBaugh, J.W., Winter, T.C., & Rosenberry, D.O. (1998). Hydrologic functions of prairie wetlands. *Great Plains Research*, *8*(1), 17–37.

Lane, C.R., & D'Amico, E. (2010). Calculating the ecosystem service of water storage in isolated wetlands using LiDAR in North Central Florida, USA. *Wetlands*, *30*(5), 1–11. http://dx.doi.org/10.1007/s13157-010-0085-z.

Lee, S. -Y., Ryan, M.E., Hamlet, A.F., Palen, W.J., Lawler, J.J., & Halabisky, M. (2015). Projecting the hydrologic impacts of climate change on montane wetlands. *PloS One*, *10*(9). http://dx.doi.org/10.1371/journal.pone.0136385.

Leibold, M.A., Holyoak, M., Mouquet, N., Amarasekare, P., Chase, J.M., Hoopes, M.F., ... Gonzalez, A. (2004). The metacommunity concept: A framework for multi-scale community ecology. *Ecology Letters*. http://dx.doi.org/10.1111/j.1461-0248.2004.00608.x.

Liu, H., Yin, Y., Piao, S., Zhao, F., Engels, M., & Ciais, P. (2013). Disappearing lakes in semiarid Northern China: Drivers and environmental impact. *Environmental Science & Technology*, *47*(21), 12107–12114. http://dx.doi.org/10.1021/es305298q.

McFeeters, S.K. (1996). The use of the Normalized Difference Water Index (NDWI) in the delineation of open water features. *International Journal of Remote Sensing*, *17*(7), 1425–1432. http://dx.doi.org/10.1080/01431169608948714.

Mitsch, W.J., & Gosselink, J.G. (2007). *Wetlands* (4th ed.). Hoboken, N.J.: Wiley.

Morris, W.F., Pfister, C.A., Tuljapurkar, S., Haridas, C.V., Boggs, C.L., Boyce, M.S., ... Menges, E.S. (2008). Longevity can buffer plant and animal populations against changing climatic variability. *Ecology*, *89*(1), 19–25. http://dx.doi.org/10.1890/07-0774.1.

Murkin, H.R., Murkin, E.J., & Ball, J.P. (1997). Avian habitat selection and prairie wetland dynamics: A 10-year experiment. *Ecological Applications*, *7*(4), 1144–1159. http://dx.doi.org/10.1890/1051-0761(1997)007[1144:AHSAPW]2.0.CO;2.

Nichol, J.E., & Vohora, V. (2004). Noise over water surfaces in Landsat TM images. *International Journal of Remote Sensing*. http://dx.doi.org/10.1080/01431160310001618770.

Niemuth, N.D., Estey, M.E., Reynolds, R.E., Loesch, C.R., & Meeks, W.A. (2006). Use of wetlands by spring-migrant shorebirds in agricultural landscapes of North Dakota's drift prairie. *Wetlands*. http://dx.doi.org/10.1672/0277-5212(2006)26[30:UOWBSS]2.0.CO;2.

Niemuth, N.D., Wangler, B., & Reynolds, R.E. (2010). Spatial and temporal variation in wet area of wetlands in the Prairie Pothole Region of North Dakota and South Dakota. *Wetlands*, *30*(6), 1053–1064. http://dx.doi.org/10.1007/s13157-010-0111-1.

Ozesmi, S.L., & Bauer, M.E. (2002). Satellite remote sensing of wetlands. *Wetlands Ecology and Management*, *10*(5), 381–402. http://dx.doi.org/10.1023/A:1020908432489.

Poiani, K.A., Johnson, W.C., Swanson, G., & Winter, T.C. (1996). Climate change and northern prairie wetlands: Simulations of long-term dynamics. *Limnology and Oceanography*, *41*, 871–881. http://dx.doi.org/10.4319/lo.1996.41.5.0871.

Reschke, J., & Hüttich, C. (2014). Continuous field mapping of Mediterranean wetlands using sub-pixel spectral signatures and multi-temporal Landsat data. *International Journal of Applied Earth Observation and Geoinformation*, *28*, 220–229. http://dx.doi.org/10.1016/j.jag.2013.12.014.

Richardson, J.J., & Moskal, L.M. (2014). Assessing the utility of green LiDAR for characterizing bathymetry of heavily forested narrow streams. *Remote Sensing Letters*, *5*(4), 352–357. http://dx.doi.org/10.1080/2150704X.2014.902545.

Rover, J., Wylie, B.K., & Ji, L. (2010a). A self-trained classification technique for producing 30 m percent-water maps from Landsat data. *International Journal of Remote Sensing*, *31*(8), 2197–2203. http://dx.doi.org/10.1080/01431161003667455.

Rover, J., Wylie, B.K., & Ji, L. (2010b). A self-trained classification technique for producing 30 m percent-water maps from Landsat data. *International Journal of Remote Sensing*, *31*(8), 2197–2203. http://dx.doi.org/10.1080/01431161003667455.

Ryan, M.E., Palen, W.J., Adams, M.J., & Rochefort, R.M. (2014). Amphibians in the climate vice: Loss and restoration of resilience of montane wetland ecosystems in the Western US. *Frontiers in Ecology and the Environment*, *12*, 232–240. http://dx.doi.org/10.1890/130145.

Sener, E., Davraz, A., & Sener, S. (2010). Investigation of Aksehir and Eber lakes (SW Turkey) coastline change with multitemporal satellite images. *Water Resources Management*, *24*, 727–745. http://dx.doi.org/10.1007/s11269-009-9467-5.

Shanmugam, P., Ahn, Y. -H., & Sanjeevi, S. (2006). A comparison of the classification of wetland characteristics by linear spectral mixture modelling and traditional hard classifiers on multispectral remotely sensed imagery in southern India. *Ecological Modelling*, *194*(4), 379–394. http://dx.doi.org/10.1016/j.ecolmodel.2005.10.033.

Song, C., Woodcock, C.E., Seto, K.C., Lenney, M.P., & Macomber, S.A. (2001). Classification and change detection using Landsat TM data: When and how to correct atmospheric effects? *Remote Sensing of Environment*, *75*(2), 230–244. http://dx.doi.org/10.1016/S0034-4257(00)00169-3.

Snodgrass, J. W., Komoroski, M. J., Bryan, A. L., & Burger, J. (2000). Relationships among isolated wetland size, hydroperiod, and amphibian species richness: Implications for wetland regulations. *Conservation Biology*, *14*(2), 414–419. http://dx.doi.org/10.1046/j.1523-1739.2000.99161.

Tavernini, S., Mura, G., & Rossetti, G. (2005). Factors influencing the seasonal phenology and composition of zooplankton communities in mountain temporary pools. *International Review of Hydrobiology*, *90*(4), 358–375. http://dx.doi.org/10.1002/iroh.200510801.

Team, R. (2013). R Development Core Team. *R: A language and environment for statistical computing*, *55*, 275–286 Retrieved from http://www.mendeley.com/research/r-language-environment-statistical-computing-96/\npapers2://publication/uuid/A1207DAB-22D3-4A04-82FB-D4DD5AD57C28

Tiner, R. (1990). Use of high-altitude aerial-photography for inventorying forested wetlands in the United-States. *Forest Ecology and Management*, *33-4*(1-4), 593–604.

Tiner, R. (2009). *Status report for the national wetlands inventory program 2009.* VA: Arlington.

Tuljapurka, S. (1990). *Population dynamics in variable environments.* New York: Springer.

USDA-FSA Aerial Photography Field Office (2006). *NAIP_1-1_1n_s_wa017_2006_1.* Utah: Salt Lake City.

USDA-FSA Aerial Photography Field Office (2011). *NAIP_2011_3ft_color_wsps_83h_img.* Utah: Salt Lake City.

Werner, B., Johnson, W.C., & Guntenspergen, G.R. (2013). Evidence for 20th century climate warming and wetland drying in the North American Prairie Pothole Region. *Ecology and Evolution*, *3*(10), 3471–3482. http://dx.doi.org/10.1002/ece3.731.

Winter, T.C. (2000). The vulnerability of wetlands to climate change: A hydrologic landscape perspective. *Journal of the American Water Resources Association*, *36*(2), 305–311 (Retrieved from <Go to ISI>://000087115000006).

Woodward, R.T., & Wui, Y.S. (2001). The economic value of wetland services: A meta-analysis. *Ecological Economics*, *37*(2), 257–270. http://dx.doi.org/10.1016/S0921-8009(00)00276-7.

Wulder, M.A., Hall, R.J., Coops, N.C., Steven, E., & Franklin, S.E. (2014). High spatial resolution remotely sensed data for ecosystem characterization*54*(6), 511–521. http://dx.doi.org/10.1641/0006-3568(2004)054[0511:HSRRSD]2.0.CO;2.

Wyawahare, M.V., Patil, P.M., & Abhyankar, H.K. (2009). Image registration techniques : An overview. *International Journal of Signal Processing, Image Processing and Pattern Recognition*, *2*(3), 11–28.